ISSN: 2754-4966

Journal of Nanosciences Research & Reports

SCIENTIFIC Research and Community

Research Article

Open Access

Synthesis and Characterization of Zinc Telluride Quantum Dots: Studies on the Structural and Optical Properties

Sharon Kiprotich

Department of Physical and Biological Sciences, Murang'a University of Technology, Murang'a, Kenya

ABSTRACT

Zinc telluride (ZnTe) quantum dots (QDs) prepared via a facile one-pot synthetic route is hereby reported. Zinc acetate, l-cysteine and potassium telluride were utilized as the starting materials for synthesis under low growth temperature (90oC) in open air conditions. The optical and structural properties of the ZnTe QDs were investigated using various analytical equipment of analysis. ZnTe photoluminescence (PL) spectra displayed a re-shift in the emission wavelength as the reaction time progressed to longer durations of growth. An increase in the emission peak intensity was observed up to 30 min of growth where a decline was observed. Ultra-visible spectroscopy analysis confirmed the red shift of the absorption edges as the reaction time increases. The optical band gap of ZnTe QDs was observed to have an inverse relation with the growth time. Structural and morphological properties were studied using X-ray diffractometer and scanning electron microscope and high resolution scanning microscope. The results were used to estimate the particle sizes which confirmed to be in the nano-range at QD levels.

Corresponding author

Sharon Kiprotich, Department of Physical and Biological Sciences, Murang'a University of Technology, P.O BOX 75-10200, Murang'a, Kenya.

Received: August 31, 2023; **Accepted:** September 06, 2023; **Published:** September 25, 2023

Keywords: Quantum Dots, Synthesis time, Zinc telluride, Structural Properties, Photoluminescence

Introduction

Semiconductor at nanoscale, otherwise referred to as quantum dots (QDs) are nanocrystals that display unusual size-dependent structural, morphological, optical and electronic properties, due to the quantum confinement of the charge carriers [1-3]. Due to the aforementioned peculiar characteristics of these materials, QDs remain to be the best promising substitutes for photoactive molecular species which are extensively being investigated for various applications that include but not limited to bio-imaging, chemo- and biosensing, opto-electronic devices, medical therapy and solar cells [4-12]. As compared to the organic chromophores, QDs have proven to posses tunable photoluminescence (PL) spectra which are dependent on the QD sizes with broad excitation spectra and narrow emission bandwidths which allow the excitation of QDs of varying colors by using a single-wavelength laser source. Moreover, it is of great importance to note that QDs possess high photo-bleaching value that permits them to be endlessly utilized for longer period of time in monitoring of biological processes. Owing to the flexibilty of the QD's surface characteristics, the same surface coating approach can be employed to conjugate QDs of any color to the desired bio-recognition molecules for in vitro and in vivo targeted delivery [13-15]. These novel characteristics of QDs make them very striking nanoprobes for a variety of biomedical applications [16-23]. Zinc telluride (ZnTe) is a group II–VI semiconductor with a room temperature direct band gap of 2.4 eV, low a□nity (3.53 eV) and an exciton bohr radius of ~7nm. There has been increased distress over the toxicity of cadmium and cadmium-based chalcogenides which have resulted in many research groups exploring other various alternative metals and/or compounds that are less toxic, large band gape, size tunable, high quantum yield, good optical properties such as zinc chalcogenides, especially ZnTe [24-26]. There are several reported synthesis methods for preparing ZnTe quantum dots, and these methods can be broadly categorized into two main approaches: colloidal synthesis and chemical vapor deposition (CVD). The colloidal synthesis method include injection method, hydrothermal synthesis, solvothermal among others while the the CVD methods include several approaches like metalorganic, laser ablation, electrochemical, biosynthesis just to mention a few [27, 28]. ZnTe QDs were synthesized using a simple one-pot synthesis technique where all the synthesis parameters were carefully controlled. This method was settled upon after series of considerations because synthesis method chosen affect features like the QD size, shape, surface properties that determine the application of the ZnTe QDs. Simple one-pot synthesis method has various advantages like its simplicity of synthesis, inexpensive nature and ability to produce monodispersed ZnTe QDs which opens its candidature to various applications like bioimaging, biolabelling, drug delivery and for possible solar cell applications as well [11,27,29].

In the recent past, synthesis of size-tunable ZnTe QDs was prepared by tailoring the band gap of alloyed QDs without altering the particle size [30,31]. However, this ability has only been used to mitigate the problem associated with extremely small (<2 nm)

QD nanocrystals, which are unstable in device applications [32]. To mitigate the stability issue, various stabilizing agents have been proposed for use as capping/stabilizing agents during synthesis. These include L-cyteine, thioglycolic acid, mercaptocarboxylic acids, poly (acrylic acid) etc [30]. L-cysteine was chosen for synthesis since it is readily available, cheap, soluble in water and can easily be absorbed into human body since it is part of the amino groups in proteins.

This research study hereby describes the size-controlled synthesis and characterization of ZnTe QDs. Various parameters such as growth time, pH, and molar ratio of the precursor solutions among others affect the core of the ZnTe hence its properties are also affected. The ability to engineer the material properties of ZnTe QDs opens a wide window of research in determining the best QD candidate for bioimaging applications. Detailed study on the morphological, structural, optical and photoluminescence properties of ZnTe QDs at varying refluxing growth time is hereby reported.

Experimental Procedure

Anhydrous Zinc acetate, potassium tellurite, L-cysteine and sodium borohydride were all of analytical grade and therefore used without any further purification in this experiment. ZnTe QDs were prepared using a procedure in ref [33,34] with a few modifications as follows: 0.5 mmol of $Zn(CH_3COO)_2.2H_2O$ was dissolved into 80 ml of deionized water in a round bottom flask. This was then followed by the addition of 0.06 g of L-cysteine with modification of pH of the solution to 11 by dropwise addition of 1M NaOH solution. After mixing for about 10 min, 0.1 mmol of K_2TeO_3 dissolved in 80 ml of deionized water and was added to the precursor solution containing zinc and L-cysteine. Upon stirring for another 5 min, 200 mg of NaBH4 was then added into the new precursor solution. The solution turned from colorless to light grey on addition of NaBH4. The reaction was left for about 5 min under stirring after which the solution was transferred to a three-necked flask attached to a condenser under heat and the nanocrystals were allowed to grow at 90° C under open air condition. The reflux reaction was monitored via aliquots taken at different time intervals of 15, 30, 60, 180, 300 and 420 minutes. These aliquots were analyzed by recording the UV/Vis absorption and PL spectra for each aliquot. As the growth time progressed from 15 to 420 min, the color of the QDs were observed to change from light grey to dark grey and finally to black.

The hot samples were then cooled down to room temperature before cleaning them several times using methanol or acetone to precipitate and centrifuged before he solvent was discarded to obtain the solid nanocrystals. The cleaned QDs were then dried in an oven at 37°C for further analysis.

The as-prepared ZnTe QDs were carefully analyzed using various analytical equipment like high resolution transmission electron microscopy (HRTEM), energy-dispersive spectroscopy (EDS), and X-ray powder diffraction (XRD) for structural and composition analysis while UV–Vis reflection and photoluminescence (PL) spectra for the ZnTe solution were measured at room temperature with a Nicolet evolution 100 UV-Vis spectrophotometer and a Nanolog Horiba JOBYN YVOWN spectrometer, respectively.

Results and Discussion

Morphological Analysis

High resolution transmission electron microscope (HRTEM) was used to analyze the surface morphology and the structure of the ZnTe QDs. Figure 1 shows HRTEM images for the ZnTe QDs grown at various reaction times. Various images were analyzed for each sample with at least 50 representative particles used to estimate their particle size and size distribution. L-cyteine was used during the synthesis to act as a capping agent. This will ensure that more stable and monodisperse ZnTe QDs are produced with little or no agglomeration. This is evident from the HRTEM results (Figure 1) where the surface morphology presents ZnTe quantum dots that are well distributed over the surface. HRTEM images (Figure 1(i)) display rod-like ZnTe QDs. ZnTe QDs formed gradually increased in size with increase in growth time. The obtained average size of the QDs estimates closely to the average value of the crystallite size calculated from the XRD pattern. The images (ii) and (iv) in Figure 1 show clear lattice fringes of the as prepared ZnTe QDs therefore indicating that the QDs formed are highly crystalline.

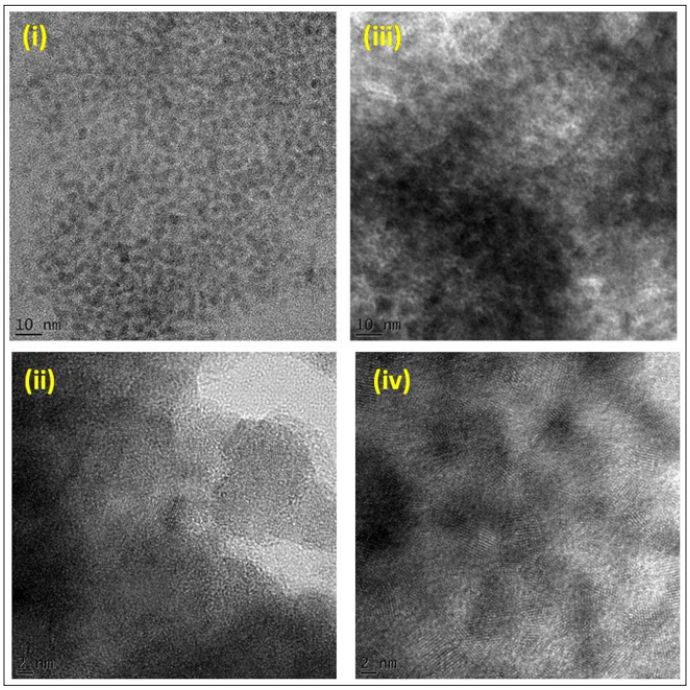

Figure 1: Representative HRTEM images for the ZnTe QDs Synthesized Various Refluxing growth time (i) & (ii) – 15 min and (iii) & (iv)- 30 min for different Magnification.

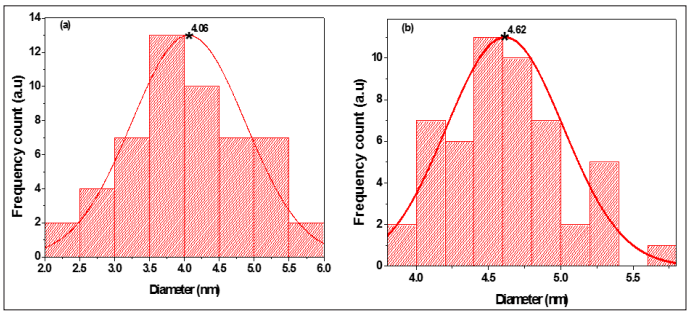

Figure 2: Histogram graphs of HRTEM images for ZnTe QDs at (a) 15 min and (b) 30 min Refluxing growth time.

Figure 2 displays the histogram graph showing the estimated particle size of the as prepared ZnTe QDs at 15 and 30 minutes of refluxing growth time. It was noted that the particle size estimates at 4.06 nm and 4.62 for samples refluxed at 15 and 30 min respectively. An increase in the particle diameter and length of the QDs were noted as the reaction time increased. This is evident in the HRTEM images displayed in Figure 1. The elemental composition of the ZnTe QDs carried out using EDS displayed a non-stoichiometric ratio where the expected elements

were present in the sample as shown in Figure 3. Other elements like C, Cu, O and S were from the sample holder or precursor solution which could not be eliminated completely during the cleaning process.

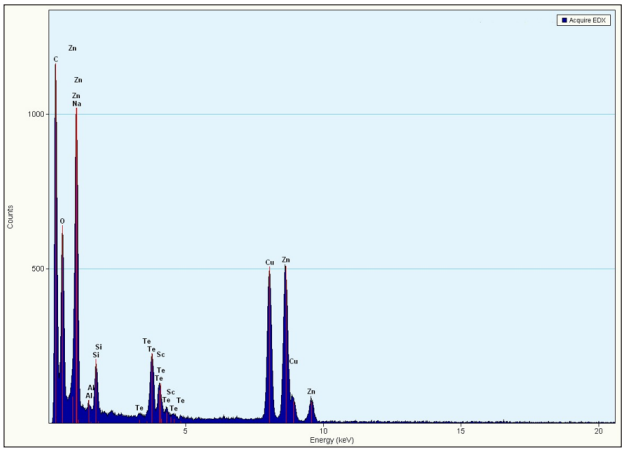

Figure 3: Representative EDS Spectrum Pattern for ZnTe QDs Prepared at 30 min of Refluxing growth time.

Structural Analysis using XRD Measurements

X-ray diffractometer is used to study the crystal structure of the ZnTe QDs and also to estimate the crystallte sizes as well as phase identification. XRD pattern for the as-prepared ZnTe QDs samples grown at various reaction time is shown in Figure 4.

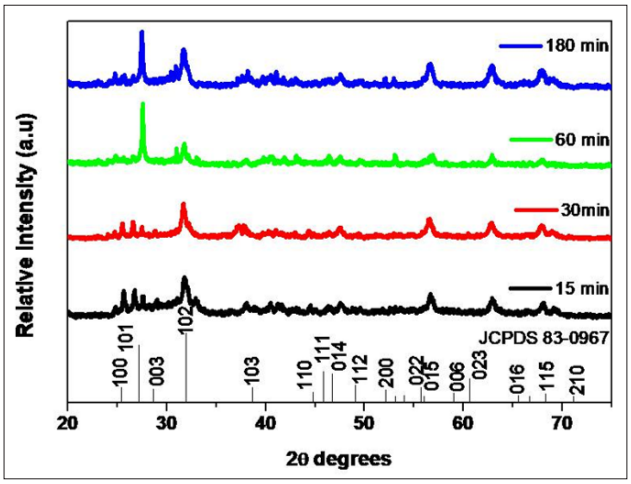

Figure 4: Representative XRD Pattern for ZnTe QDs Prepared at Varying Refluxing growth times

The XRD pattern display wurtzite (hexagonal) crystal structures for all the as-prepared samples refluxed at various reaction times. The bars at the bottom represents the bulk wurtzite structure of ZnTe as indicated in the standard card (JCPDS No. 82-2152). The XRD peaks were observed to decrease in the size of the full width at half maximum (FWHM) and shifted to lower 2thetha angles as ZnTe QDs grew with increase in reaction time.

The crystallite sizes for ZnTe QDs were calculated using the Scherrer's formula (Eq.1) [35].

$$D = \frac{0.9\,\lambda}{\beta\,\cos\theta_B}$$

Where λ, θ and β are the X-ray wavelength (1.54056 Å), Bragg's diffraction angle and average diffraction peak full width at half maximum of the ZnTe QDs respectively. The estimated size of the crystals of the ZnTe QDs increased from 15.69 to 23.07 nm as the growth time progressed to longer durations of growth from 15 to 180 min. The discrepancy observed from the crystallite sizes obtained from XRD and particle size could be due to the fact that several particles could form a crystal. This could also be attributed to agglomeration of QDs at longer growth time which affects the size estimates of the ZnTe QDs. There was also an observation of an inverse relation between the XRD peaks broadening with refluxing growth time.

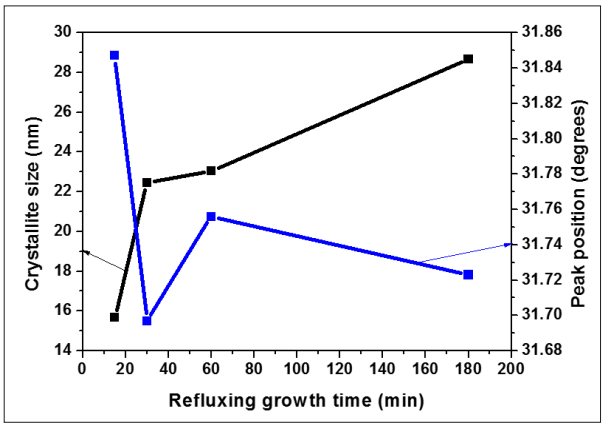

Figure 5: Variation in the Crystallite Sizes and Peak Position of ZnTe QDs for Various Refluxing growth times.

Figure 5 shows how the particle size of the ZnTe QDs progressively increased with increase in reaction time as displayed by the narrow peak width of the XRD spectra at longer reflux time. The diffraction peak positions of the XRD spectra shift slightly to lower 2θ angle with increasing growth time; this is demonstrated by the dominant peak shifting from 36.35 to 36.21 degrees for growth time 15 to 180 minutes respectively as shown in Figure 4. This phenomenon is associated with the increase in the crystallite size of ZnTe QDs. The peak intensity however increased slightly at 30 minutes of refluxing growth time and decreased thereafter (Figure 6). Maximum diffraction peak intensity was observed for growth time 30 minutes. This depicts a most crystalline and mono-disperse ZnTe QD sample obtained at 30 min of growth. This is because as the particle increases in size, the quality of the crystallite is enhanced to a certain optimum time of growth where the preferred orientations of the grains become well defined. FWHM decreased with increasing growth time due to the increase in the average crystallite sizes of the ZnTe QDs. It can also be attributed to Ostwald ripening where smaller particles merge to form larger particles [36].

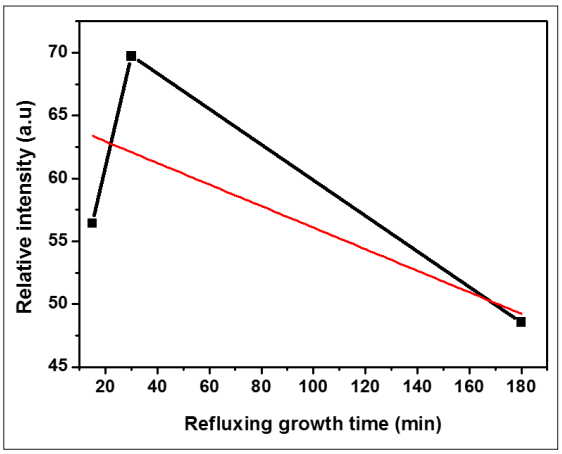

Figure 6: A Graph of Changes in Peak Intensity and Linear fit of ZnTe QDs as a Function of Refluxing growth time

Photoluminescence Analysis

Figure 7 (a) display the emission spectra obtained from the PL analysis of ZnTe QDs samples at varying reaction time.

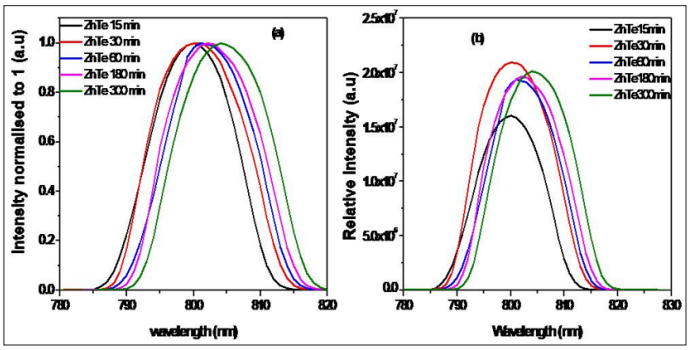

Figure 7: (a) Normalized and (b) as-Prepared PL Emission Spectra of ZnTe QDs Synthesized at different Reaction times (15, 30, 60,180 and 300min).

The dependence of the emission peak of the QDs on the reaction time was evident from the study. The absorption band was seen to shift to longer wavelength for longer refluxing growth time. This is believed to be due to enlargement of the QD sizes. In varying the reaction time from 15-300 minutes the ZnTe QDs luminescent emission peak was generally red shifted from approximately 799 nm to 804 nm. Figure 7 (b) however shows changes in the peak intensity as growth time increased from 15 to 300 minutes. Highest intensity was observed at 30 minutes of refluxing growth time.

All the samples prepared possessed well-resolved absorption maxima related to the first electronic transition. This observation indicates the satisfactorily narrow size distribution of the QDs. This observed absorption maxima shift to the higher wavelength as the size of the QDs enlarged due to the effects of quantum confinement. These observations were confirmed in Figure 8 by the shift and the colour of emission as the QDs grow even at longer durations of growth. The constricted emission spectra observed from the as-prepared ZnTe QDs points to nearly monodisperse and homogeneous state of the QDs. Yu et.al 2003 [37], discussed a method of calculating the particle sizes of the QDs using the first absorption peak using the following empirical formula eqn. 2;

$$D = \left(9.8127\times10^{-7}\right)\lambda^3 - \left(1.7147\times10^{-3}\right)\lambda^2 + \left(1.0064\right)\lambda - 194.84 \quad (2)$$

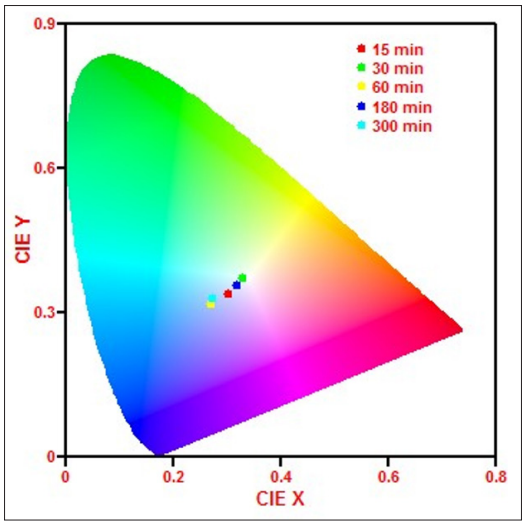

Figure 8: A CIE Image for the As-Prepared ZnTe QDs obtained from the PL Emission Spectra

Where λ is the first absorption maximum wavelength of the as-prepared ZnTe QDs. The results showed that the mean diameters of the as prepared ZnTe QDs are15.27 nm (15min), 15.39 nm (30min), 15. 64 nm (60 min), 15.66 nm (180min) and15.96 nm (300 min) corresponding with PL peaks of 799.9, 800.7, 802.4, 802.8 and 804.5nm which are in agreement with XRD observation.

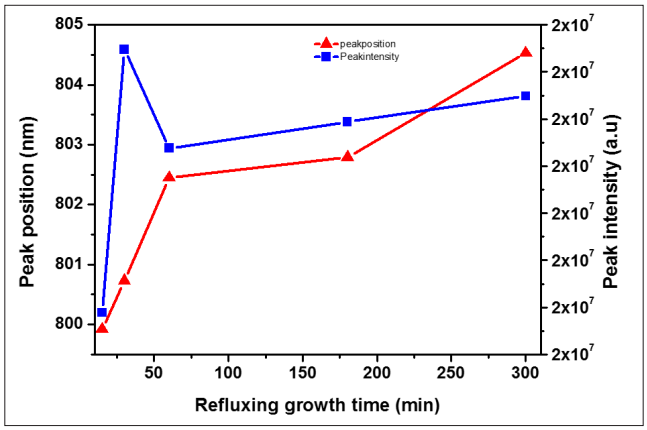

Figure 9: PL Graph Showing Changes in Peak Position and Intensity of ZnTe QDs with Increase in Refluxing growth time of Synthesis from 15 to 300 min

Figure 9 displays how peak position and intensity of as synthesized ZnTe QDs are affected by the refluxing growth time. Peaks shift to longer wavelength from approximately 799 to 804 nm for reaction time between 15min and 300 min indicating growth of the particle sizes. From the graph, the intensity rises rapidly at 30 min, drops and rises again gradually as the reaction time progresses. The general increase in the intensities with increase in refluxing growth time shows an increase in the crystallinity of the ZnTe QDs [38-40].

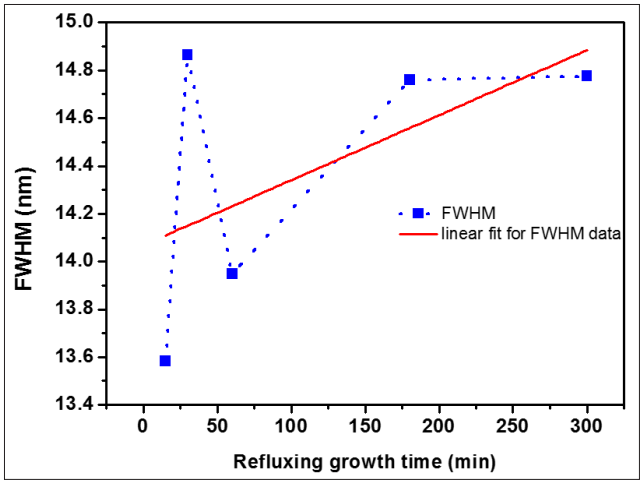

Figure 10: A Linear fit of PL Bandwidth at different Reaction times (15, 30, 180 and 300 min) of ZnTe QDs.

Figure 10 demonstrates how the bandwidth of PL spectra increases linearly as the growth time increases. This could be due to increase in ZnTe quantum dots as reaction progresses. The PL bandwidth is observed to increases gradually as larger ZnTe NPs are formed. The bandwidth is mostly presided over by the non-uniform enlargement from the size distribution of the sample. This occurrence is regular with the Ostwald ripening process where the QDs that are larger in size emit light at longer wavelength. Full width at half maximum of the PL spectra is observed to broaden as the reaction progresses.

Optical Properties

Difference in slope and absorption edges is observed for as synthesized ZnTe QDs. As displayed by Figure 11, the inception of band edge absorption was established to be red shifted with increasing particle size confirming the sized dependent absorption properties of ZnTe NPs. The energy band gap of ZnTe was projected by means of Kubelka-Munk emission equation [33, 41], for direct evolutions. It was observed that the energy band gap reduced from 2.27 to 2.01 eV as the growth of the QDs progressed for longer durations of growth as shown in Figure 12

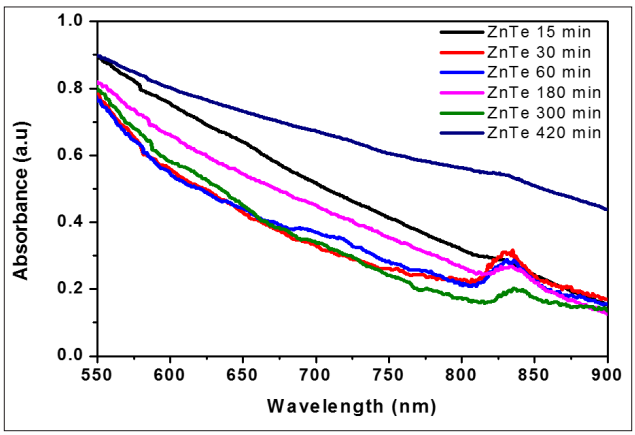

Figure 11: The Absorbance Spectra of ZnTe QDs Grown at Various Reflux Time

Absorption spectra red-shifts upon increase in refluxing growth time of ZnTe QDs samples. The size distribution becomes narrower after synthesizing at various reaction times compared to the bulk ZnTe. The absorption edges of ZnTe samples were in the range of 825 - 836 nm. The approximated band gap is; however, smaller than that of the bulk ZnTe (2.26 eV). The observed reduction in the energy band gap could be attributed to the surface defects density of undoped ZnTe [24, 42].The slope of the different samples prepared varied due to the non-uniformity in particle sizes as confirmed by HRTEM analysis.The E values for the ZnTe nanoparticles were calculated by extrapolating the linear portion of the $(khv)^2$ verses hv curves to the hv axis (Figure 12). The E values for ZnTe prepared at 15, 30, 60, 180, 300 and 420 minutes were 2.27, 2.20, 2.19, 2.17, 2.16 and 2.01 eV respectively.

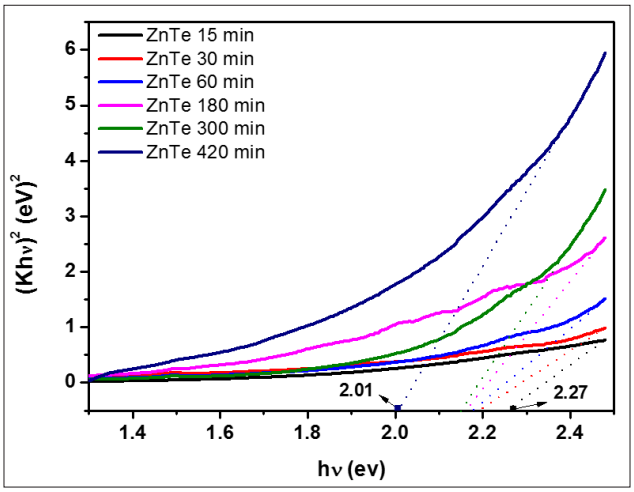

Figure 12: Graphical Plot Showing Variation in The Band Gap Energy of the As-Prepared Znte Quantum Dots At Different Reflux Time.

Conclusion

ZnTe QDs were successfully synthesized using a single apparatus to produce QDs with a range of morphologies and sizes. Powerful near-infrared emissions were observed from the ZnTe QDs synthesized at 300 minutes which could be attributed by the increased size of the ZnTe QDs. PL analysis showed a red shift (799-804nm) in the emission band followed by a continuous increase in the intensity as reaction progresses from 15 to 300 minutes. It also displayed a narrow size distribution of the nanoparticles as indicated by PL bandwidth of 13.58 to 14.77 nm for various reflux time. Spherical ZnTe QDs with fairly good mono-dispersion and average diameters increasing as refluxing growth time increases were observed. The XRD pattern for different refluxing growth time was found to be wurtzite (hexagonal) with predominant (002) peak. It was realized that the calculated sizes of the crystallites using the Scherrer equation enlarged from 15.69 to 23.07 nm with increase in refluxing growth time from 15 to 180 min. This could be observed and realized through the narrowing of the X-ray diffraction peaks at extended refluxing growth time. The as prepared ZnTe QDs at 180 minutes synthesis time was found to be more crystalline than that at 15 minutes. The electronic properties obtained from the UV-Visible radiation analysis displayed reduction in the band gap from 2.27 to 2.01 eV with increasing refluxing growth time. The obtained properties of ZnTe QDs make them good candidates for biological applications.

Declaration of Conflict of Interest

There is no conflict of interest to declare.

Acknowledgement

The author acknowledges the support by University of the Free State, South Africa in running analysis for the samples prepared.

References

1. CB Murray, CR Kagan, MG Bawendi (2000) Synthesis and Characterization of Monodisperse Nanocrystals and Close-Packed Nanocrystal Assemblies. Annu Rev Mater Sci 30: 545-610.
2. Victor I Klimov (2012) Semiconductor and Metal Nanocrystals, ed Dekker, New York, https://www.taylorfrancis.com/books/edit/10.1201/9780203913260/semiconductor-metal-nanocrystals-victor-klimov.
3. AL Rogach (2008) Semiconductor Nanocrystal Quantum Dots. Springer-Verlag Wien https://link.springer.com/book/10.1007/978-3-211-75237-1.
4. J Callan, AP De Silva, RC Mulrooney, BM Caughan (2007) Luminescent Sensing with Quantum Dots. J Incl Phenom Macrocycl Chem 58: 257-262.
5. RC Somers, MG Bawendi, DG Nocera (2007) CdSe nanocrystal based chem-/bio- sensors. Chem Soc Rev 36: 579.
6. R Gill, M Zayats, I Willner (2008) Semiconductor quantum dots for bioanalysis. Angew Chem Int Ed 47: 7602-7625.
7. R Freeman, I Willner (2012) Optical molecular sensing with semiconductor quantum dots (QDs). Chem Soc Rev 41: 4067-4085.
8. N Hildebrandt (2011) Biofunctional Quantum Dots: Controlled Conjugation for Multiplexed Biosensors. ACS Nano 5: 5286-5290.
9. TL Doane, C Burda (2012) The unique role of nanoparticles in nanomedicine: imaging, drug delivery and therapy. Chem Soc Rev 41: 2885-2911.
10. DV Talapin, J-S Lee, MV Kovalenko, EV Shevchenko (2010) Prospects of Colloidal Nanocrystals for Electronic and Optoelectronic Applications. Chem Rev 110: 389-458.

11. PV Kamat, K Tvrdy, DR Baker, JG Radich (2010) Beyond Photovoltaics: Semiconductor Nanoarchitectures for Liquid-Junction Solar Cells. Chem Rev 110: 6664-6688.
12. S Ruhle, M Shalom, A Zaban (2010) Quantum-Dot-Sensitized Solar Cells. PhysChem 11: 2290-2304.
13. M Bruchez, Jr, M Moronne, P Gin, S Weiss, A P Alivisatos (1998) Semiconductor nanocrystals as fluorescent biological labels. Science 281: 2013-2016.
14. X Gao, Y Cui, R M Levenson, L W K Chung, S Nie (2004) In vivo cancer targeting and imaging with semiconductor quantum dots. Nat Biotech 22: 969-976.
15. WC Chan, S Nie (1998) Quantum dot bioconjugates for ultrasensitive nonisotopic detection. Science 281: 2016-2018.
16. SJ Byrne, SA Corr, TY Rakovich, YK Gun'ko, YP Rakovich, et al. (2006) Optimisation of the synthesis and modification of CdTe quantum dots for enhanced live cell imaging. J Mat Chem 16: 2896-2902.
17. R Cui, HC Pan, JJ Zhu, HY Chen (2007) Versatile Immunosensor Using CdTe Quantum Dots as Electrochemical and Fluorescent Labels. Anal Chem 79: 8494-8501.
18. Z Deng, Y Zhang, J Yue, F Tang, Q Wei (2007) Green and orange CdTe quantum dots as effective pH-sensitive fluorescent probes for dual simultaneous and independent detection of viruses. J Phys Chem B 111: 12024-12031.
19. WC Law, KT Yong, I Roy, G Xu, H Ding, et al. (2008) Optically and Magnetically Doped Organically Modified Silica Nanoparticles as Efficient Magnetically Guided Biomarkers for Two-Photon Imaging of Live Cancer Cells. J Phys Chem C 112: 7972-7977.
20. KT Yong, J Qian, I Roy, HH Lee, EJ Bergey, et al. (2007) Quantum rod bioconjugates as targeted probes for confocal and two-photon fluorescence imaging of cancer cells. Nano Lett. 7: 761-765.
21. WT Al-Jamal, KT Al-Jamal, PH Bomans, PM Frederik, K Kostarelos (2008) Functionalized-Quantum-Dot–Liposome Hybrids as Multimodal Nanoparticles for Cancer. Small 4: 1406-1415.
22. L Shi, B Hernandez, M Selke (2006) Singlet Oxygen Generation from Water-Soluble Quantum Dot−Organic Dye Nanocomposites. J Am Chem Soc 128: 6278-6279.
23. G Xu, KT Yong, I Roy, SD Mahajan, H Ding, et al. (2008) Bioconjugated quantum rods as targeted probes for efficient transmigration across an in vitro blood-brain barrier. Bioconjugate Chem 19: 1179-1185.
24. B Wana, C Hua, B Fenga, J Xua, Y Zhanga, et al. (2010) Optical properties of ZnTe nanorods synthesized via a facile low-temperature solvothermal route. Mater Sci Eng B 171: 11-15.
25. P Christian, E Liu (2010) Low temperature synthesis of metal chalcogenide nanoparticles in mesitylene. Polyhedron 29: 691-696.
26. M Bruchez Jr, M Moronne, P Gin, S Weiss, A P Alivisatos (1998) Semiconductor Nanocrystals as Fluorescent Biological Labels. Science 281: 2013-2016.
27. Ouyang J, Christopher I Ratcliffe, David Kingston, Baptiste Wilkinson, Jamijin Kuijper, et al. (2008) Gradiently alloyed ZnxCd1−xS colloidal photoluminescent quantum dots synthesized via a noninjection one-pot approach. J Phys Chem C 112: 4908-4919.
28. Patra Sovan Kumar, Bhavya Bhushan, Amiya Priyam (2016) Water-soluble, luminescent ZnTe quantum dots: supersaturation-controlled synthesis and self-assembly into nanoballs, nanonecklaces and nanowires. Dalton Transactions 45: 3918-3926.
29. Patra Sovan Kumar, Bhavesh Kumar Dadhich, Bhavya Bhushan, Ravi Kant Choubey, Amiya Priyam (2021) Nonlinear absorption and refraction of highly monodisperse and luminescent ZnTe quantum dots and their self-assembled nanostructures: implications for optoelectronic devices. ACS omega 46: 31375-31383.
30. Oluwasesan Adegoke, Enoch Y Park (2016) Size-confined fixed-composition and composition-dependent engineered band gap alloying induces different internal structures in L-cysteine-capped alloyed quaternary CdZnTeS quantum dots. Scientific reports 6: 27288.
31. R E Bailey, Nie S (2003) Alloyed semiconductor quantum dots: tuning the optical properties without changing the particle size. J Am Chem Soc 125: 7100-7106.
32. M D Regulacio, M D Han (2010) Composition-tunable alloyed semiconductor nanocrystals. Accounts Chem Res 43: 621-630.
33. Kiprotich S, Dejene FB, Ungula J, Onani MO (2016) The influence of reaction times on structural, optical and luminescence properties of cadmium telluride nanoparticles prepared by wet-chemical process. Physica B Condensed Matter 480: 125-30.
34. Ungula J, Kiprotich S, Swart HC, Dejene BF (2022) Investigation on the material properties of ZnO nanorods deposited on Ga□doped ZnO seeded glass substrate: Effects of CBD precursor concentration. Surface and Interface Analysis 54: 1023-1031.
35. RS Wagner, C Doherty (1996) J Electroceram Soc 113 1300 3 4596.
36. KK Nanda, FE Kruis, H Fissan, (2002) Evaporation of free PBS nanoparticles: evidence of the Kelvin effect. Phys Rev Lett 89: 256103.
37. WW Yu, L Qu, W Guo, X Peng (2003) Experimental Determination of the Extinction Coefficient of CdTe, CdSe, and CdS Nanocrystals. Chem Mater 15: 2854-2860.
38. S Kim, B Fisher, HJ Eisler, MG Bawendi (2003) Type-II Quantum Dots: CdTe/CdSe(Core/Shell) and CdSe/ZnTe(Core/Shell) Heterostructures. J Am Chem Soc 125: 11466-11467.
39. CY Chen, CT Cheng, CW Lai, YH Hu, PT Chou, et al. (2005) Type-II CdSe/CdTe/ZnTe (Core–Shell–Shell) Quantum Dots with Cascade Band Edges : The Separation of Electron (at CdSe) and Hole (at ZnTe) by the CdTe Layer. Small 1: 1215-1220.
40. D Dorfs, A Salant, I Popov, U Banin (2008) ZnSe Quantum Dots Within CdS Nanorods: A Seeded-Growth Type-II System. Small 4: 1319-1323.
41. I Shalish, H Temkin, V Narayana (2004) Size-dependent surface luminescence in ZnO nanowires. Phys Rev B 69: 245401.
42. Kiprotich S, Dejene B F, Onani M O (2018) Structural, optical and luminescence properties of CdTe quantum dots: Investigation on the effect of capping ligand ratio. Materials Research Express 5: 065028.